Saudi Journal of Biological Sciences 27 (2020) 3258–3266

Contents lists available at ScienceDirect

Saudi Journal of Biological Sciences

journal homepage: www.sciencedirect.com

Original article

Exposure of rainbow trout (*Oncorhynchus mykiss*) to magnetite (Fe_3O_4) nanoparticles in simplified food chain: Study on ultrastructural characterization

Nargiz J. Agayeva [a], Fuad H. Rzayev [b,c], Eldar K. Gasimov [b], Chingiz A. Mamedov [a,*], Ismat S. Ahmadov [a], Narmina A. Sadigova [a], Ameer Khusro [d,*], Naif Abdullah Al-Dhabi [e], Mariadhas Valan Arasu [e]

[a] Department of Zoology of Vertebrates, Faculty of Biology, Baku State University, Baku AZ1148, Azerbaijan
[b] Laboratory of Electron Microscopy of the SRC, Azerbaijan Medical University, Baku AZ1078, Azerbaijan
[c] Institute of Zoology, National Academy of Sciences, Baku AZ1004, Azerbaijan
[d] Research Department of Plant Biology and Biotechnology, Loyola College, Chennai 600034, Tamil Nadu, India
[e] Department of Botany and Microbiology, College of Science, King Saud University, P.O. Box 2455, Riyadh 11451, Saudi Arabia

ARTICLE INFO

Article history:
Received 26 July 2020
Revised 13 September 2020
Accepted 15 September 2020
Available online 23 September 2020

Keywords:
Aquatic ecosystem
Bioaccumulation
Fe_3O_4 nanoparticles
Microscopic analyses
Oncorhynchus mykiss

ABSTRACT

The widespread exposure of metallic nanoparticles to the aquatic ecosystem and its adverse impact on human life is the colossal concern worldwide. In view of this, this context was investigated to analyze microscopically the bioaccumulation and localization of magnetite (Fe_3O_4) nanoparticles in the cellular organelles of rainbow trout (*Oncorhynchus mykiss*, Walbaum, 1792) in aquatic conditions. Initially, Fe_3O_4 nanoparticles were absorbed on to Elodea (*Elodea canadensis*) and fed to molluscs (*Melanopsis praemorsa*). Fish were fed with the same molluscs, and then the intestines and liver were examined using light and transmission electron microscopy. Results showed that nanoparticles were present in the cytoplasm and other organelles of cells (mitochondrion and lysosome) by absorbing through microvilli of the epithelial cells of the tunica mucosa in the intestine. Further, nanoparticles passed through the vessels of the lamina propria of the tunica mucosa and reached to the sinusoids of the liver via blood circulation. It was then accumulated from the endothelium of the sinusoid to the cytoplasm of liver hepatocytes and to mitochondria and lysosome. The accumulation of nanoparticles in the epithelial cells, cytoplasm, mitochondria, and lysosome revealed the degree of transparency of the pattern with slight hesitation. In summary, this investigation contributed towards the understanding of the physiological effects of Fe_3O_4 nanoparticles on *O. mykiss*, which ascertains essentiality for sustainable development of nanobiotechnology in the aquatic ecosystem.

© 2020 The Author(s). Published by Elsevier B.V. on behalf of King Saud University. This is an open access article under the CC BY-NC-ND license (http://creativecommons.org/licenses/by-nc-nd/4.0/).

1. Introduction

In view of the advancement in nanotechnology sector, the applications of nanomaterials in disparate industries have grown rapidly over the past few years. Metallic nanoparticles are widely used in biomedical, food, agriculture, and electronic industries due to their unique physico-chemical attributes (Prakash et al., 2016; Arul et al., 2017; Reddy et al., 2018; Magdalane et al., 2019; Kaviyarasu et al., 2020). Also, previous studies showed that nanomaterials-based antioxidant therapies have an important role against environmental induced oxidative stress (Eftekhari et al., 2018). Iron oxide nanoparticles, particularly magnetite (Fe_3O_4) are one of the extensively used metallic nanomaterials in pharmaceutical and agricultural industries due to their super paramagnetic properties (Remya et al., 2015). In addition, studies also reported its versatile role in the remediation of soil and groundwater, removal of pollutants from water, treatment of chlorinated solvents, and prevention of dental caries (Lei et al., 2018). Unfortunately, the enormous release of Fe_3O_4 nanoparticles in the environment and its uncontrolled toxicity for the aquatic

* Corresponding authors.
E-mail addresses: m_chingiz@yahoo.com (C.A. Mamedov), armankhan0301@gmail.com (A. Khusro).

Peer review under responsibility of King Saud University.

Production and hosting by Elsevier

https://doi.org/10.1016/j.sjbs.2020.09.032
1319-562X/© 2020 The Author(s). Published by Elsevier B.V. on behalf of King Saud University.
This is an open access article under the CC BY-NC-ND license (http://creativecommons.org/licenses/by-nc-nd/4.0/).

ecosystem are the colossal concern. As a matter of fact, iron oxide nanoparticles are known to enter the water via effluent discharge and pose a significant risk to aquatic organisms. Recent studies reported toxicity of iron oxide nanoparticles in diversified aquatic animals viz. *Danio rerio* (Zheng et al., 2018), *Labeo rohita* (Remya et al., 2015), *Oncorhynchus tshawytscha* (Srikanth et al., 2017), *Daphnia magna* (Keller et al., 2012), *Brachionus rotundiformis* (Mashjoor et al., 2018), and *Artemia salina* (Zhu et al., 2017). However, the toxicity assessment of iron oxide nanoparticles on other aquatic animals is scarce or still undetermined.

Rainbow trout (*Oncorhynchus mykiss*, Walbaum, 1792) is one of the most important fishes grown widely worldwide for diversified commercial purposes (Ahmadov et al., 2018a). Metal oxides nanoparticles easily pass physiological barriers causing glutathione depletion, lipid peroxidation, lysosomal/mitochondrial toxicity, and subsequently apoptosis and mutations (Kaloyianni et al., 2020; Radwan et al., 2020). Prior investigations demonstrated that nanoparticles had altered the physiological and biochemical traits of *O. mykiss* by affecting its vital organs. The exposure of titanium dioxide nanoparticles showed certain biochemical changes in the brain of *O. mykiss* (Ramsden et al., 2009). Likewise, the dose-dependent toxicity of carbon nanotubes caused alterations in the rate of ventilation and gill pathologies of *O. mykiss* (Smith et al., 2007). In general, metallic nanoparticles interact with the aquatic ecosystem at different stages of the life cycle and change the biochemical balance of the organisms (Xia et al., 2013). Current studies indicate that effect of iron oxide nanoparticles in the living system is not completely benign. Toxicities of these nanoparticles are species-dependent mechanism which certainly emphasizes to understand their detrimental impact on the aquatic ecosystem (Ates et al., 2016). Thus, in order to assess further the toxicity of iron oxide nanoparticles on the aquatic organism and fill the gap of the research, the present context was investigated to evaluate the effect of Fe_3O_4 (20–30 nm) nanoparticles into the food chain and analyze its possible bioaccumulation in various cellular organelles of *O. mykiss* at the ultrastructural level.

2. Materials and methods

2.1. Food chain design

The first component of the food chain in this investigation was Elodea (*Elodea canadensis*; Family - Hydrocharitaceae) aquatic plant. This plant plays an important role in the formation and stability of ecosystems in both saltless and marine water basins. The plant plays the role of habitats of invertebrates, insects, and fishes in the water, organizes their nutritional resources, weakens water movement, accelerates the deposition of dust, soil, and clay particles in the water, and promotes the movement of nutrients in the food chain.

Freshwater snail (*Melanopsis praemorsa*; Family – Melanopsidae) was used as the second component of the food chain in this study. The water environment must be rich in oxygen for the snail's survival and normal growth. Therefore, these snails grow better and generate in the phytoplankton-rich waters. *M. praemorsa* is mainly fed by small-scale fractions with extracts of green algae. When stored in the aquarium, they have an active movement. Hence, this snail species was chosen for this investigation.

At different stages of the experiment, 1-year old *O. mykiss* females (13.26 ± 0.15 g) were obtained from Gabala fish farm (Gabala city, Azerbaijan) and maintained in Institute of Zoology of ANAS (Baku city, Azerbaijan). The length, mass, fullness, cavity fertility, and sexual maturity coefficients of fries and sires used in the experiment were determined according to the methodology of ichthyology (Emre and Kürüm, 2007).

2.2. Duration of study

The main phase of the research was conducted from January 2017 to March 2018 at the Gabala salmon farming factory, Republic of Azerbaijan. Experiments were carried out as per the approval from the Ethics Committee of Azerbaijan Medical University (Ministry of Health of Azerbaijan Republic).

2.3. Nanoparticles used

Magnetite (Fe_3O_4) nanoparticles (purity 98%) of 20–30 nm in size were purchased from Skyspring Nanomaterials Inc., USA. Stock solutions (0.1% w/v) of Fe_3O_4 nanoparticles were prepared by mixing its appropriate amount in sterile double distilled water.

2.4. Nanoparticles exposure design

The toxicity of Fe_3O_4 nanoparticles exposure to *O. mykiss* was designed as per the methodology of Ahmadov et al. (2018a). Initially, *E. canadensis* was kept in 0.1% (w/v) aqueous solution of Fe_3O_4 nanoparticle for 3 days. Nanoparticles were thus adsorbed on the surface of the plant and were accumulated in the stem, leaves, and other organs. *O. mykiss* was fed with *M. praemorsa* containing Fe_3O_4 nanoparticles, which was also fed with *E. canadensis*. Experiments were carried out in 3 aquariums (1 control and 2 tests) with 60 L of water. The temperature of water was set between 10 and 12 °C while pH was maintained between 7.6 and 8.2. Each aquarium contains six fish. In the control aquarium, *O. mykiss* was fed with molluscs separated from shells. In the test aquarium, *O. mykiss* was fed with molluscs which were fed earlier with *E. canadensis*. Daily feeding ration constituted ~10% of body mass for 3 days. After the finishing period, morphology as well as the anatomy of internal organs (intestines and liver) of *O. mykiss* was observed.

2.5. Microscopic analyses of tissues and nanoparticles bioaccumulation analysis

O. mykiss from the control and the test aquariums were sacrificed and the abdominal area was dissected using a sterile scalpel. Araldite-Epon blocks were made from materials using general methods (Kuo, 2007). The semi-thin (1–2 μm) sections from the blocks took on EM UC7 (Leica, Germany) ultra-microtome, stained with methylene blue, azure II, and mainly with a fixer or toluidine blue were observed under light microscope Primo Star (Zeiss, Germany) and images of required portions were shot with EOS D650 (Canon, China) digital camera (D'Amico, 2005).

Prepared and unstained sections of 50–70 nm thickness from the same blocks were studied on JEM-1400 (JEOL, Japan) transmission electron microscope (TEM) at a voltage of 80–120 kV and electronograms were made. The intestine and liver of each fish were taken and fixed in 0.1 M phosphate buffer (pH – 7.4) containing 2.5% glutaraldehyde, 2% paraformalaldehyde, 4% sucrose, and 0.1% picric acid. The fixed samples were observed under TEM. Samples were post fixed in 1% osmium tetraoxide solution within 2 h after being left in the same fixer for one day. The morphometric analysis of the image was performed on electronograms using the computer program. The TEM imaging platform was developed by Soft Imaging Solutions Gmbh (Olympus, Germany).

The histograms obtained during the study of electronograms were taken from ultra-thin sections made of non-stained preparations by "Intensity Profile" computer software. The length (nm) of structures drawn in horizontal direction and the digits showing

gray color patterns in the vertical direction (grey value) were provided. It should be noted that the intensity of the image in the electrograms depends on the degree of gray color, the weakest intensity being black and the highest intensity represents white colour. These indicators allow determining accurately the place of accumulation of nanoparticles in the cells.

3. Results

Initially, signs for morphological changes in fish of both groups were identified. The average length and average weight of the fish in the control group were measured as 11.8 cm and 13.2 g, respectively. On the other hand, the average length and average weight of the fish in test group were measured as 12.4 cm and 16.6 g, respectively (Figure not shown).

Fig. 1A shows all the layers of the intestinal wall and lumen of *O. mykiss* observed under a light microscope. The wall of the small intestine of the rainbow trout, as in other vertebrates, is composed of mucous membranes, sub-mucosal base, muscle, and serous mucosa. The main structural element of the mucous membrane is the intestinal microvillus. Fig. 1B–D shows various layers in separate large magnifier (as shown in the scale images) and their histological structure. Fig. 1B shows that tunica mucosa itself consists of different types of cells and layers. The epithelial layer of the intestinal villus is composed of cylindrical enterocytes (indicated by stars) and goblet cells (indicated by arrows). The epithelial layer encloses a lamina propria (indicated by flowers). Fig. 1C shows the magnified image of the sub-mucous layer between the mucous and the muscular layers. Fig. 1D shows muscle and serous layers of the intestinal wall. Images of the semi and ultrathin sections obtained in this context clearly showed that there was a layer of muscle. Ultra-structurally, the apical surface of enterocytes (shown in Fig. 1C and D) facing the intestinal mouth contains cytoplasmic protrusions - microvilli, which repeatedly increases the absorption surface. The latter combines with the glycocalyx cover to form a marginal edge, which is also visible under a light microscope. In the apical part of the outer surfaces of enterocytes, intercellular connections are formed in the presence of dense, adhesive, and desmosomes (indicated by arrowheads in Fig. 1D). It should be noted that there is a terminal web composed of cortical cytoskele-

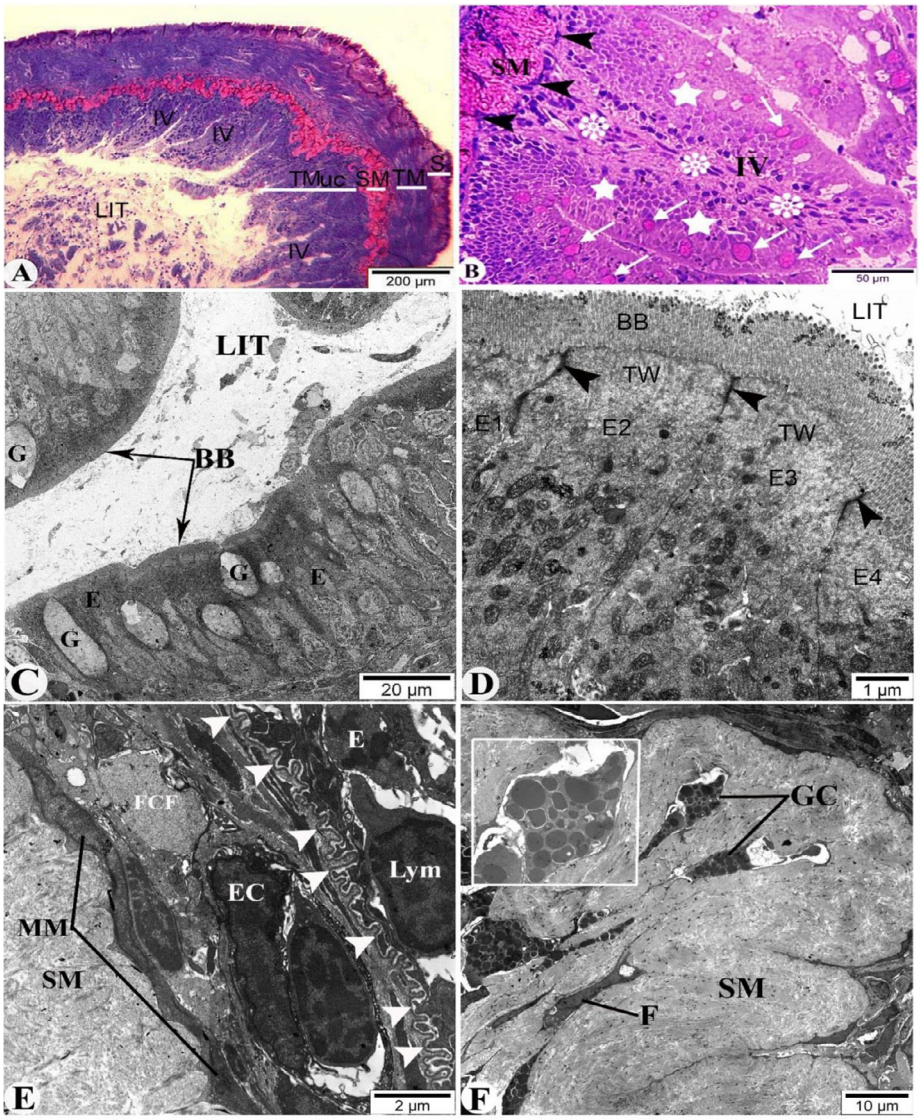

Fig. 1. Light-optical (A-B) and ultrastructural (C-F) characteristics of the small intestinal wall of *O. mykiss.* BB – brush border; E – enterocyte; EC – endothelial cell; FCF – fascicle collagen fibers; G – goblet cell; GC – granular cells; IV – intestinal villus; LIT – lumen intestine tenue; Lym – lymphocytes; MM – muscularis mucosae; S – serosa; SM – sub-mucosa; TMus – tunica mucosa; TM – tunica muscularis; TW – terminal web.

tal elements and organelles dominated by mitochondria in the apical parts of the cytoplasm of enterocytes. As shown in Fig. 1D, the bulk of the sub-cellular the base consists of bundles of type III collagen fibres with a diameter of less than 70 nm. Results include fibrocytes and granular cells. The enlarged form of osmophilic granules of granular cell framed in Fig. 1D suggests that the shape and structure of mammals are similar to those of obstructed cell granules. It should be noted that during the trichrome staining of semi-thin sections, staining of glycoproteins enclosing type III collagen fibres, glycosaaminoglycans, and cellular elements included in the structure of main substance in the form of bright fuchsinophilic stripes causes a sharp difference of sub-mucosal base from the surrounding structures. Between the basal surface of the enterocytes and the special surface elements of the surrounding villi, there is a continuous basal surface. Starting from the basal surface of the enterocytes, lymphocytes are located between the enterocytes at different levels (Fig. 1E).

Electron microscopic image of the muscle layer in the mucosa of the intestinal wall of *O. mykiss* is illustrated in Fig. 2. In fractions perpendicular to the longitudinal axis of the small intestine, the muscular cord located directly around the sub-mucosal base is composed of a circular layer of internal circular smooth muscle cells (Fig. 2B) and a circular outer longitudinal plain muscle cells (Fig. 2B) consist of an organized longitudinal layer. Between the layers of the muscular membrane of the small intestine are structures belonging to the myoentorial nerve and vascular sheaths, surrounded by elements of connective tissue (indicated by snowflakes in Fig. 2A and B). These sheaths, along with the muscular membrane, are involved in the nourishment and innervations of other muscles. The surface of the small intestine facing the peritoneal cavity is covered with a serous membrane surrounded by mesothelial cells belonging to the single-layered squamous epithelium. Structurally, the trout contains a special layer of serous membrane in the serous layer (between the mesothelial cells and the superficial longitudinal plain muscle cells) composed of connective tissue elements (Fig. 2C).

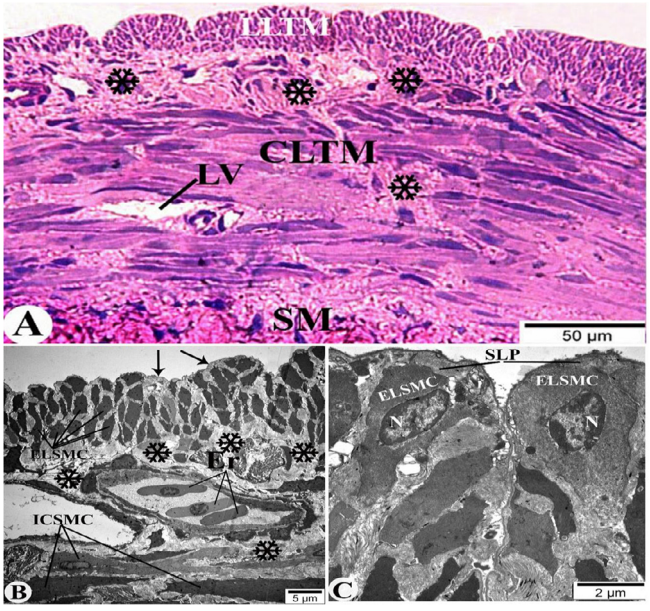

Fig. 2. Structural elements of the muscular and serous membranes of the small intestine of *O. mykiss*. A – semi-thin section stained by methylene blue, azure II and fuchsin, B and C – electronograms of ultra-thin sections stained by uranyl acetate and pure lead citrate. CLTM – circular layer tunica muscularis; ELSMC – external longitudinal smooth muscle cell; Er – erythrocytes; ICSMC – internal circular smooth muscle cell; LLTM – longitudinal layer tunica muscularis; LV – lymphatic vessels; N – nucleus; SLP – serosal lamina propria; SM – sub-mucosa.

The structure (layers) of the intestinal wall of *O. mykiss* was also observed under TEM. Changes in the structures involved in the formation of the small intestinal wall of trout under the influence of Fe_3O_4 nanoparticles are presented in Fig. 3A. Fig. 3A illustrates the mucous and sub-mucous layers of the intestinal wall which showed goblet and epithelial cells. The electrogram shows an increase in the number of enterocytes in the wall of the small intestine, the nuclei of which are deformed to varying degrees, and the number of mononuclear cells surrounded by unpainted areas on all sides. At the marginal edges of the apical surfaces of enterocytes, there is a significant reduction in the number of microvilli compared to the control. In addition, a large number of myelin-like structures were also observed in the immediate vicinity of the villi. Fig. 3B shows the epithelial cells, goblet cells, lamina propria, and microvilli. In the enlarged form of the marginal edge (Fig. 3B), it is clear that myelin-like structures are directly related to the plasmolemma surrounding the microvilli. In conclusion, it should be noted that under the influence of Fe_3O_4 nanoparticles, along with various changes in the wall of the small intestine, there is a violation of the integrity of the phospholipid layer of membrane structures.

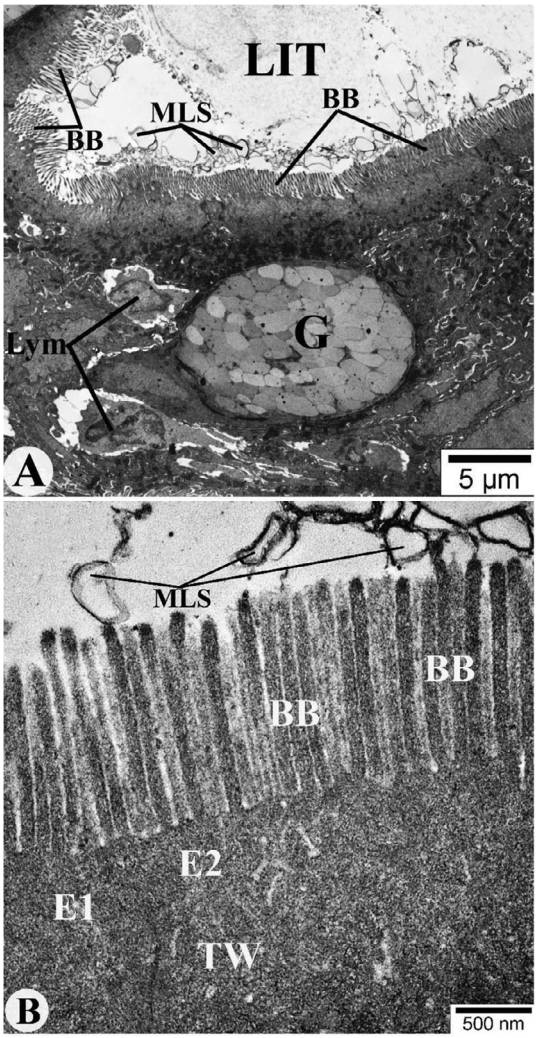

Fig. 3. Ultrastructural characteristics of changes in the structural elements of the wall of the small intestine (**A**) and the apical part enterocytes (B) of *O. mykiss* under the influence of Fe_3O_4 nanoparticles. BB – brush border; E – enterocyte; G – goblet cell; LIT – lumen intestine tenue; Lym – lymphocytes; MLS – myelin-like structures; TW – terminal web.

The movement and accumulation of Fe_3O_4 nanoparticles in *O. mykiss* was observed using TEM. The TEM analysis showed the penetration of Fe_3O_4 nanoparticles into the epithelial cells of mucosa of the intestine (Fig. 4A) as well as diffusion in their cytoplasm (Fig. 4B). In addition, Fe_3O_4 nanoparticles were also found within the mitochondria and lysosomes (Fig. 4C and D). The accumulation of nanoparticles in the epithelial cells, cytoplasm, mitochondria, and lysosome is shown in Fig. 4E–H which revealed the degree of transparency of the pattern with little hesitation (5600–5650).

Fig. 5A and B exhibit the passage of nanoparticles through the basal membrane of the epithelial layer of the tunica mucosa to the connective tissue being in lamina propria, the endothelium of vessels, and finally to erythrocytes (Fig. 5A and B). The degree of transparency of the pattern was revealed with slight hesitation (5600–5650) in the intestine (Fig. 5C and D).

Light microscopic images of semi-thin sections of the fish liver (1 μm) are presented in Fig. 6A which clearly showed hepatocytes, sinusoids, and veins. Fig. 6A shows a central vein containing a large number of blood-forming elements with a wide lumen in the classical hepatic lobule. Sinusoidal capillaries are located between the hepatic trabeculae around the central vein. In addition, TEM images of the indicated liver sections are presented in Fig. 6B. Significant changes in hepatocytes under the influence of Fe_3O_4 nanoparticles are the detection of symptoms characteristic of steatosis in the peripheral parts of the classic particles (Fig. 6C and D). Ultrastructurally, granular osmophilic remnants and myelin-like structures are found in the lumen of steatotic vacuoles located in the cytoplasm of hepatocytes. In addition, due to the action of nanoparticles in the cytoplasm of hepatocytes, ribosomes are separated in granular endoplasmic reticulum cisterns and the amount of secondary lysosomes is increased. The fact that the diameters of steatotic vacuoles are small compared to the size of the nuclei and mainly located in the periportal areas of classical particles suggests that the effect of Fe_3O_4 nanoparticles leads to the development of acute toxic microvesicular steacytosis in the liver parenchyma.

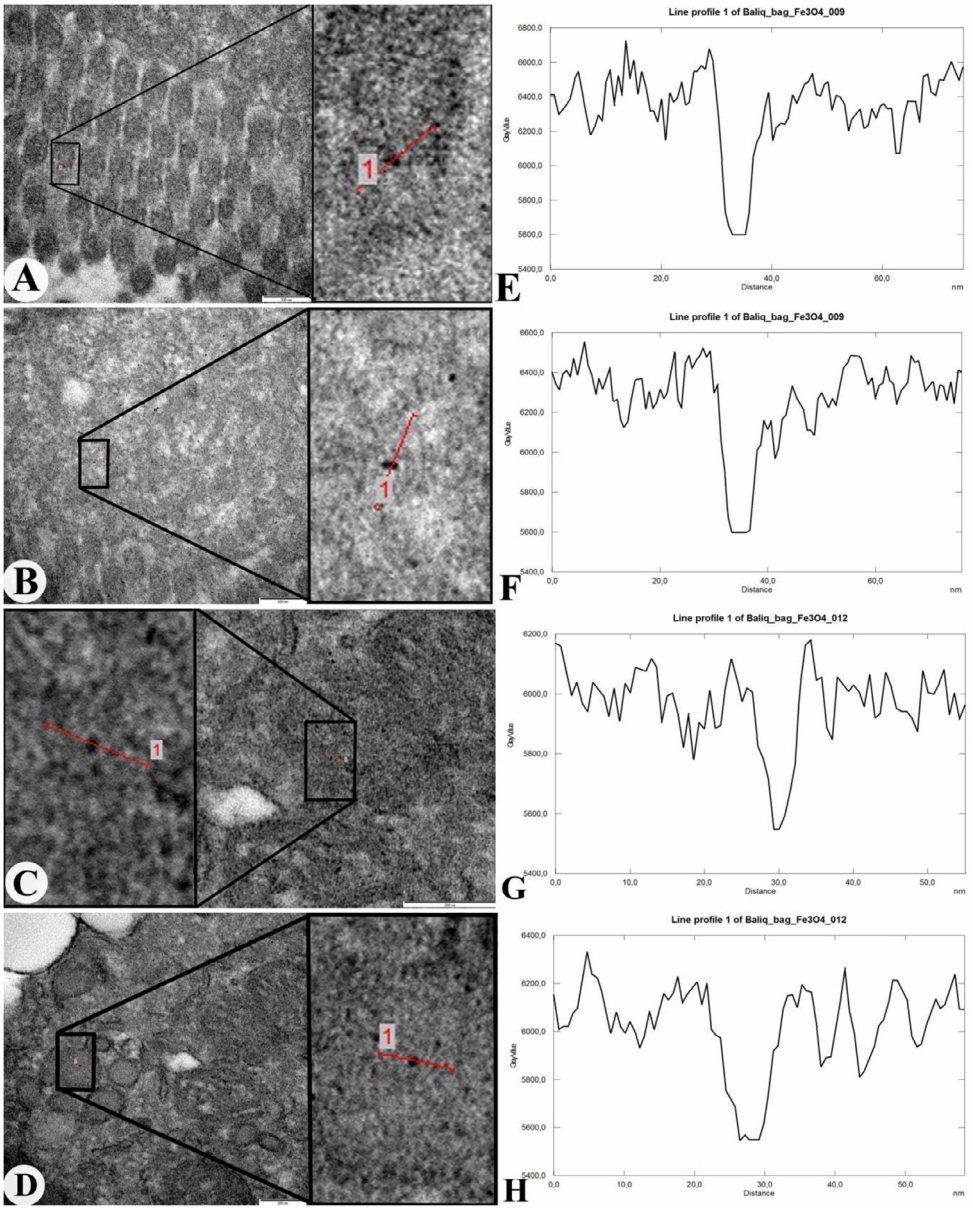

Fig. 4. TEM images of Fe_3O_4 nanoparticles accumulation in (A) epithelial cells, (B) cytoplasm, (C) mitochondria, and (D) lysosome of intestinal walls of *O. mykiss* as well as graphical representation for bioaccumulation of nanoparticles in (E) epithelial cells, (F) cytoplasm, (G) mitochondria, and (H) lysosome of intestinal walls of *O. mykiss*.

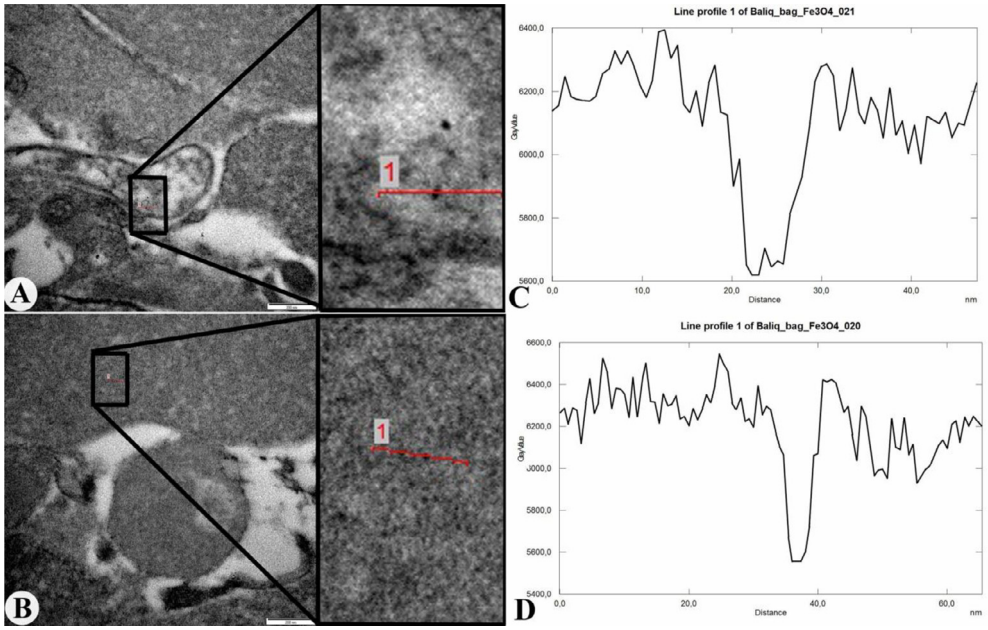

Fig. 5. TEM images of Fe_3O_4 nanoparticles accumulation in (A) endothelial cells of vessels in lamina propria and (B) erythrocytes of *O. mykiss* as well as graphical representation for bioaccumulation of nanoparticles in (C) endothelial cells of vessels in lamina propria and (D) erythrocytes of *O. mykiss*.

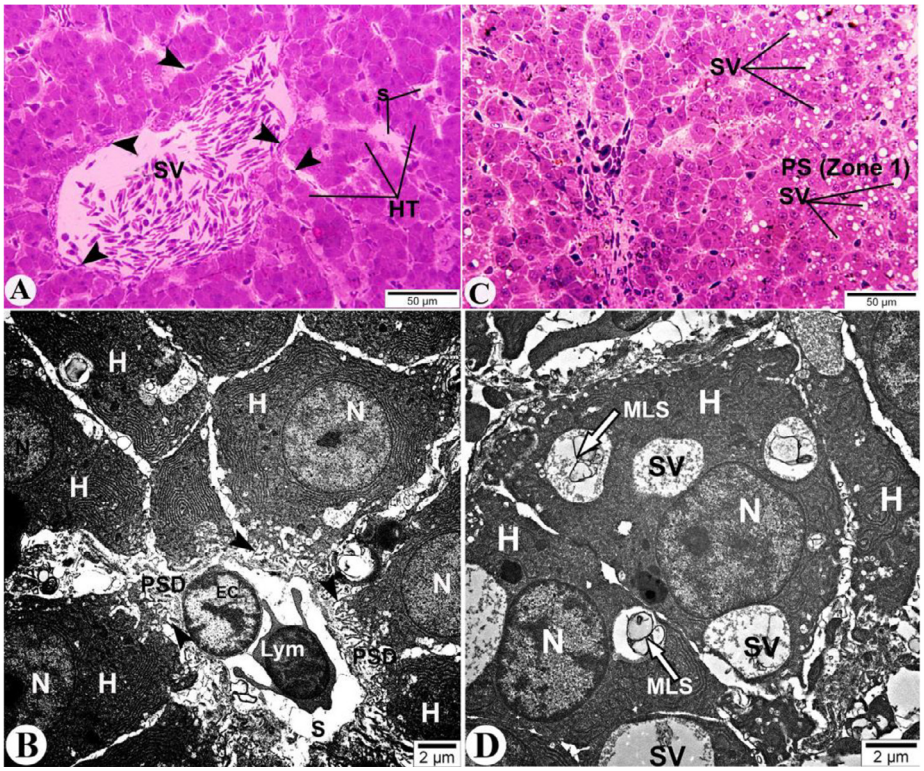

Fig. 6. Morphological characteristics of the structural elements of the liver *O. mykiss* in normal conditions (A and B) and exposure to Fe_3O_4 nanoparticles (C and D). SV – central vein; EC – endothelial cell; Er – erythrocyte; H – hepatocyte; HT – hepatic trabecula; Lym – lymphocytes; MLS – myelin-like structures; N – nucleus; PS – periportal space (zone 1); PSD – perisinusoidal space Disse; S – sinisoid; SV – steatotic vacuoles (microvesicles).

Fig. 7A shows the presence of Fe_3O_4 nanoparticles in the endothelium of the sinusoids between hepatocytes of rainbow trout's liver (Fig. 7A). Additionally, nanoparticles were found in the nucleus and cytoplasm (Fig. 7B) as well as mitochondria and lysosomes of hepatocytes (Fig. 7C and D). Thus, nanoparticles along with nutrients were absorbed through the intestines of fish and entered the blood. It then passed to the liver's hepatocytes by entering blood through sinusoids. The degree of transparency of the nanoparticles recorded in different parts of the liver of *O. mykiss* at a certain fluctuation (5250–5650) is presented in Fig. 7E–H.

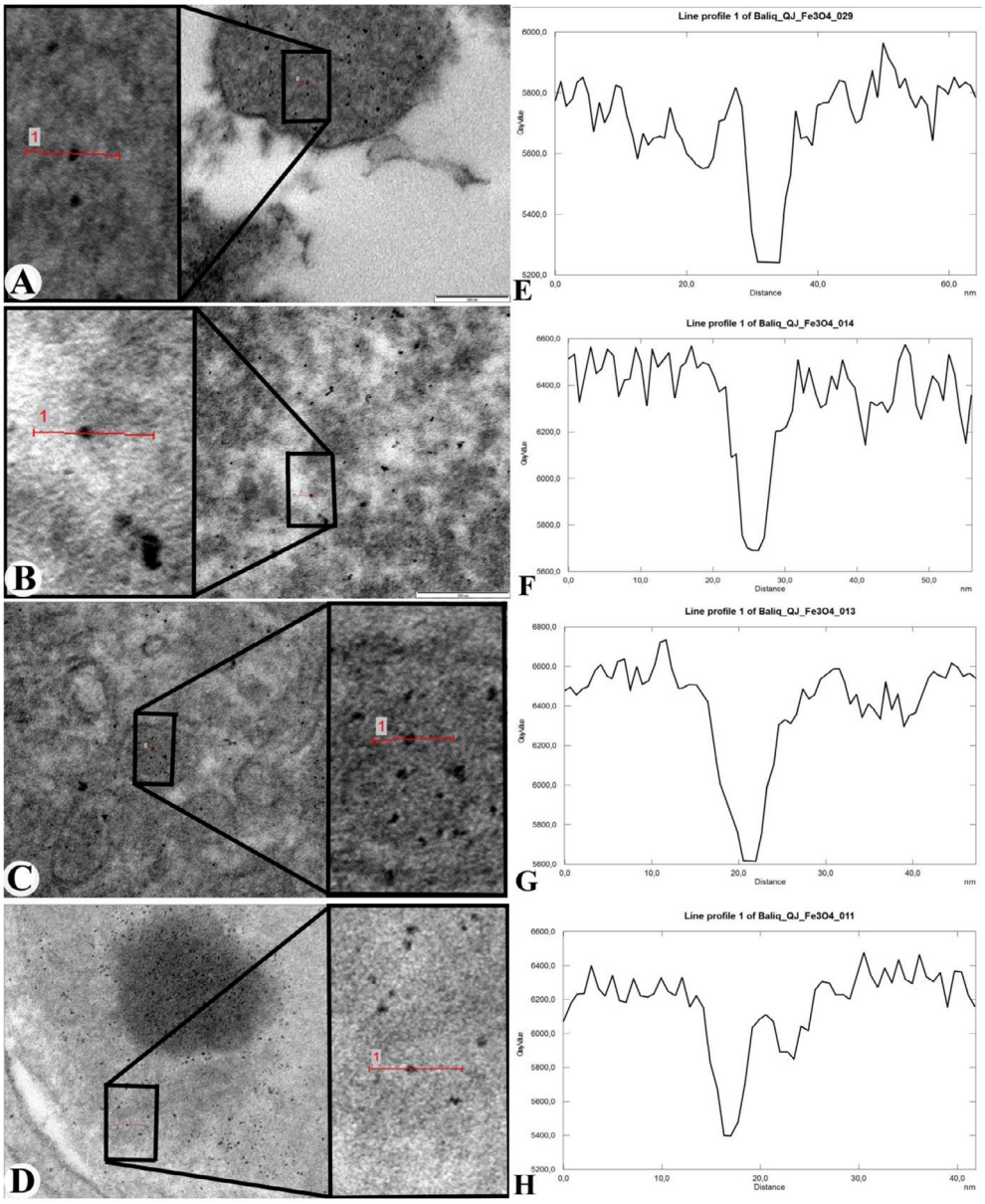

Fig. 7. TEM images of Fe_3O_4 nanoparticles accumulation in (A) endothelium of sinusoid, (B) hepatocytes, (C) mitochondria, and (D) lysosome of *O. mykiss* as well as graphical representation for bioaccumulation of nanoparticles in (E) endothelium of sinusoid, (F) hepatocytes, (G) mitochondria, and (H) lysosome of intestinal walls of *O. mykiss*.

4. Discussion

Fishes are pivotal aquatic organisms that are generally known to play a pivotal role in the food chain of the aquatic ecosystem. Due to their unique characteristics to respond against low doses of xenobiotics and accumulate various toxicants, they are considered model organisms for disparate eco-toxicological studies. The exposure of metallic nanoparticles in the aquatic system alters the morphological and physiological nature of fishes as a result of its toxicity. Therefore, bioaccumulation, distribution, and site-specific localization of toxic nanoparticles in fishes are colossal areas of interest at present.

Previously, it was shown that nanoparticles entered the first trophic level of the food chain (*E. canadensis*) and accumulated in their bodies. Detection of nanoparticles by TEM in organs of molluscs fed with plants exposed to nanoparticles revealed their transition from elodea to molluscs (Ahmadov et al., 2018a). In the present study, the exposure of Fe_3O_4 (20–30 nm) nanoparticles into the food chain of *O. mykiss* showed not only its possible bioaccumulation in various organs but also physiological alteration in the ultra-structural level. Iron-based nanoparticles have shown toxic impact on various organisms of the aquatic ecosystem in the past. Ates et al. (2016) investigated the chronic influence of Fe_2O_3 structures on the bioaccumulation, elimination, hematology, and immunological responses of *Oreochromis niloticus* which revealed immunotoxic effects along with significant reduction in serum glucose and increment in glutamic oxaloacetic transaminase, glutamic pyruvic transaminase, and lactate dehydrogenase levels. In another study, Zhu et al. (2017) demonstrated the effect of varying doses of Fe_3O_4 nanoparticles on the cyst and larval stages of *Artemia salina* and concluded its toxicity on the organisms of the aquatic ecosystem.

Mitochondria and lysosome are important source/target of free radicals and most of the disease (Ahmadian et al., 2016, 2017).

Xenobiotics-induced toxicities are related to the alterations in the function of these organelles including electron transfer chain (Fard et al., 2016). Therefore, investigation of mitochondria/ lysosomes, pro-inflammatory mediators, antioxidant defense and nuclear factor-kappa B signaling pathway as biomarkers of exposure to environmental pollutants including nanoparticles can simplify the application of a quick preventive responses in the ecosystems (Mandegary et al., 2013; Ahmadian et al., 2018; Caixeta et al., 2020; Radwan et al., 2020). In addition, endocytosis is considered as the prime mechanism for the accumulation of nanoparticles in mitochondria and lysosome of cells (Zhang et al., 2016).

In the food chain, the dispersion and transfer of nanoparticles from one trophic level to the other is mainly due to the digestive system (intestines), but there may be cases where the nanoparticles are in direct contact with the water organisms. Therefore, it is important to study the effects of nanoparticles on the organisms which form the food chain, regardless of the path they go through. Microscopic images of this context showed that Fe_3O_4 nanoparticles can accumulate in their intestines and liver after feeding *O. mykiss* with *M. praemorsa*. Results of this investigation confirmed that if fish were fed with nanoparticles-exposed *M. praemorsa*, the toxic nanoparticles could accumulate in their bodies. Ahmadov et al. (2018b) determined that Fe_3O_4 nanoparticles had a catalytic influence on spermatozoid acrosomes, accelerated the energy process, and increased the spermatozoids activities, which led to an enhancement in the fertilization rate of *O. mykiss*. In a like manner, Özgür et al. (2018) estimated significant reduction in the spermatozoa velocities of *O. mykiss* due to the exposure of Fe_3O_4 nanoparticles. In another study, Campos-Garcia et al. (2016) examined the histopathological changes in O. niloticus gills due to the exposure of carbon nanotubes. Findings illustrated dislocation as well as hyperplasia of the epithelial cells, and disarrangement of the capillaries.

5. Conclusions

In a nutshell, TEM analysis showed the bioaccumulation of Fe_3O_4 nanoparticles in various cellular organelles of *O. mykiss* and exhibited physiological alterations at ultra-structural level. Microscopic images illustrated that Fe_3O_4 nanoparticles can accumulate in the intestine and liver of *O. mykiss* after feeding with *M. praemorsa*. Since fishes are the prime sources of food for humans, the transfer of toxic nanoparticles to the human body at subsequent trophic levels may pose specific health risks. Therefore, one of the main approaches of modern nanotechnology-based ecological research will be to understand the pathways of nanoparticles passage in the food chain and identify the paramount factors influencing the mechanism for avoiding such drastic health concern.

Declaration of Competing Interest

The authors declare that they have no known competing financial interests or personal relationships that could have appeared to influence the work reported in this paper.

Acknowledgements

Authors would like to acknowledge Baku state university and Azerbaijan Medical University for the support. The authors extend their appreciation to The Researchers supporting project number (RSP-2020/20) King Saud University, Riyadh, Saudi Arabia.

References

Ahmadian, E., Eftekhari, A., Fard, J.K., Babaei, H., Nayebi, A.M., Mohammadnejad, D., et al., 2017. *In vitro* and *in vivo* evaluation of the mechanisms of citalopram-induced hepatotoxicity. Arch. Pharm. Res. 40, 1296–1313.

Ahmadian, E., Khosroushahi, A.Y., Eftekhari, A., Farajnia, S., Babaei, H., Eghbal, M.A., 2018. Novel angiotensin receptor blocker, azilsartan induces oxidative stress and NFkB-mediated apoptosis in hepatocellular carcinoma cell line HepG2. Biomed. Pharmacother. 99, 939–946.

Ahmadian, E., Pennefather, P.S., Eftekhari, A., Heidari, R., Eghbal, M.A., 2016. Role of renin-angiotensin system in liver diseases: an outline on the potential therapeutic points of intervention. Expert Rev. Gastroent. 10, 1279–1288.

Ahmadov, İ.S., Gasımov, E.K., Sadıqova, N.A., Agayeva, N.J., Rzayev, F.H., Manafov, A. A., 2018a. Transfer of nanoparticles in a simplified aquatic food chain: from water plant *Elodea canadensis* to mollusks *Lymnaea auricularia*. J. Low Dimens. Syst. 2, 41–45.

Ahmadov, I.S., Sadıqova, N.A., Agayeva, N.J., Mamedov, C.A., 2018b. Influence of nanoparticles on the yield of embryos of the roe rainbow trout (*Oncorhynchus mykiss* Walbaum) in the fermentation process. J. Oceanogr. Mar. Res. 6, 183. https://doi.org/10.4172/2572-3103.1000183.

Arul, K.T., Manikandan, E., Murmu, P.P., Kennedy, J., Henini, M., 2017. Enhanced magnetic properties of polymer-magnetic nanostructures synthesized by ultrasonication. J. Alloys Compd. 720, 395–400.

Ates, M., Demir, V., Arslan, Z., Kaya, H., Yılmaz, S., Camas, M., 2016. Chronic exposure of tilapia (*Oreochromis niloticus*) to iron oxide nanoparticles: Effects of particle morphology on accumulation, elimination, hematology and immune responses. Aquat. Toxicol. 177, 22–32.

Caixeta, M.B., Araújo, P.S., Gonçalves, B.B., Silva, L.D., Grano-Maldonado, M.I., Rocha, T.L., 2020. Toxicity of engineered nanomaterials to aquatic and land snails: a scientometric and systematic review. Chemosphere 260, 127654.

Campos-Garcia, J., Martinez, D.T., Rezende, K.F., da Silva, J.R., Alves, O.L., Barbieri, E., 2016. Histopathological alterations in the gills of *Nile tilapia* exposed to carbofuran and multiwalled carbon nanotubes. Ecotoxicol. Environ. Saf. 133, 481–488.

D'Amico, F., 2005. A polychromatic staining method for epoxy embedded tissue: a new combination of methylene blue and basic fuchsine for light microscopy. Biotech. Histochem. 80, 207–210.

Eftekhari, A., Dizaj, S.M., Chodari, L., Sunar, S., Hasanzadeh, A., Ahmadian, E., et al., 2018. The promising future of nano-antioxidant therapy against environmental pollutants induced-toxicities. Biomed. Pharmacother. 103, 1018–1027.

Emre, Y., Kürüm, V., 2007. Havuz ve Kafeslerde Alabalık Yetiştiriciliği. Posta Basım Evi, Seyrantepe, İstanbul, p. 272.

Fard, J., Hamzeiy, H., Sattari, M., Eftekhari, A., Ahmadian, E., Eghbal, M.A., 2016. Triazole rizatriptan induces liver toxicity through lysosomal/mitochondrial dysfunction. Drug Res. 66, 470–478.

Kaloyianni, M., Dimitriadi, A., Ovezik, M., Stamkopoulou, D., Feidantsis, K., Kastrinaki, G., et al., 2020. Magnetite nanoparticles effects on adverse responses of aquatic and terrestrial animal models. J. Hazard. Mater. 383, 121204.

Kaviyarasu, K., Magdalane, C.M., Jayakumar, D., Samson, Y., Bashir, A.K.H., Maaza, M., et al., 2020. High performance of pyrochlore like $Sm_2Ti_2O_7$ heterojunction photocatalyst for efficient degradation of rhodamine-B dye with waste water under visible light irradiation. J. King Saud Univ. Sci. 32, 1516–1522.

Keller, A.A., Garner, K., Miller, R.J., Lenihan, H.S., 2012. Toxicity of nano-zero valent iron to freshwater and marine organisms. PLoS One 7, e43983.

Kuo, J., 2007. Electron Microscopy: Methods and Protocols. Humana Press, Totowa. 808–625.

Lei, C., Sun, Y., Tsang, D.C.W., Lin, D., 2018. Environmental transformations and ecological effects of iron-based nanoparticles. Environ. Pollut. 232, 10–30.

Magdalane, C.M., Kaviyarasu, K., Priyadharsini, G.M.A., Bashir, A.K.H., Mayedwa, N., Matinise, N., et al., 2019. Improved photocatalytic decomposition of aqueous Rhodamine-B by solar light illuminated hierarchical yttria nanosphere decorated ceria nanorods. J Mater. Res. Technol. 8, 2898–2909.

Mandegary, A., Saeedi, A., Eftekhari, A., Montazeri, V., Sharif, E., 2013. Hepatoprotective effect of silyamarin in individuals chronically exposed to hydrogen sulfide; modulating influence of TNF-α cytokine genetic polymorphism. Daru 21, 28.

Mashjoor, S., Yousefzadi, M., Zolgharnain, H., Kamrani, E., Alishahi, M., 2018. Organic and inorganic nano-Fe_3O_4: Alga *Ulva flexuosa*-based synthesis, antimicrobial effects and acute toxicity to briny water rotifer *Brachionus rotundiformis*. Environ. Pollut. 237, 50–64.

Özgür, M.E., Ulu, A., Balcıoğlu, S., Özcan, İ., Köytepe, S., Ateş, B., 2018. The Toxicity Assessment of iron oxide (Fe_3O_4) nanoparticles on physical and biochemical quality of rainbow trout spermatozoon. Toxics 6, 62. https://doi.org/10.3390/toxics6040062.

Prakash, T., Williams, G.V.M., Kennedy, J., Rubanov, S., 2016. High spin-dependent tunneling magnetoresistance in magnetite powders made by arc-discharge. J. Appl. Phys. 120, 123905.

Radwan, M.A., El-Gendy, K.S., Gad, A.F., 2020. Biomarker responses in terrestrial gastropods exposed to pollutants: A comprehensive review. Chemosphere 257, 127218.

Ramsden, C.S., Smith, T.J., Shaw, B.J., Handy, R.D., 2009. Dietary exposure to titanium dioxide nanoparticles in rainbow trout, (*Oncorhynchus mykiss*): no effect on growth, but subtle biochemical disturbances in the brain. Ecotoxicology 18, 939–951.

Reddy, Y.S., Magdalane, C.M., Kaviyarasu, K., Mola, G.T., Kennedy, J., Maaza, M., 2018. Equilibrium and kinetic studies of the adsorption of acid blue 9 and Safranin O from aqueous solutions by MgO decked FLG coated Fuller's earth. J. Phys. Chem. Solids 123, 43–51.

Remya, A.S., Ramesh, M., Saravanan, M., Poopal, R.K., Bharathi, S., Nataraj, D., 2015. Iron oxide nanoparticles to an indian major carp, *Labeo rohita*: Impacts on hematology, iono regulation and gill Na^+/K^+ atpase activity. J. King Saud Univ. Sci. 27, 151–160.

Smith, C.J., Shaw, B.J., Handy, R.D., 2007. Toxicity of single walled carbon nanotubes on rainbow trout, (*Oncorhynchus mykiss*): respiratory toxicity, organ pathologies, and other physiological effects. Aquat. Toxicol. 82, 94–109.

Srikanth, K., Trindade, T., Duarte, A.C., Pereira, E., 2017. Cytotoxicity and oxidative stress responses of silica-coated iron oxide nanoparticles in CHSE-214 cells. Environ. Sci. Pollut. Res. 24, 2055–2064.

Xia, J., Zhao, H.Z., Lu, G.H., 2013. Effects of selected metal oxide nanoparticles on multiple biomarkers in *Carassius auratus*. Biomed. Environ. Sci. 26, 742–749.

Zhang, X., Zhang, H., Liang, X., Zhang, J., Tao, W., Zhu, X., et al., 2016. Iron Oxide nanoparticles induce autophagosome accumulation through multiple mechanisms: lysosome impairment, mitochondrial damage, and ER stress. Mol. Pharm. 13, 2578–2587.

Zheng, M., Lu, J., Zhao, D., 2018. Effects of starch-coating of magnetite nanoparticles on cellular uptake, toxicity and gene expression profiles in adult zebrafish. Sci. Total Environ. 622–623, 930–941.

Zhu, S., Xue, M.Y., Luo, F., Chen, W.C., Zhu, B., Wang, G.X., 2017. Developmental toxicity of Fe_3O_4 nanoparticles on cysts and three larval stages of *Artemia salina*. Environ. Pollut. 230, 683–691.